HHS Public Access

Author manuscript

Prostate. Author manuscript; available in PMC 2024 April 01.

Published in final edited form as:

Prostate. 2023 April ; 83(5): 416–429. doi:10.1002/pros.24474.

Conditional gene regulation models demonstrate a pro-proliferative role for growth hormone receptor in prostate cancer

Christopher J. Unterberger[1], **Sean J. Mcilwain**[2], **Philippos K. Tsourkas**[2], **Vilena I. Maklakova**[1], **Jordyn L. Prince**[1], **Abigail Onesti**[1], **Rong Hu**[3], **John J. Kopchick**[4], **Steven M. Swanson**[1], **Paul C. Marker**[1]

[1]School of Pharmacy, Pharmaceutical Sciences Division, University of Wisconsin-Madison, Madison, Wisconsin 53705, USA

[2]School of Medicine and Public Health, University of Wisconsin-Madison, Madison, Wisconsin 53705, USA

[3]School of Medicine and Public Health, Department of Pathology and Laboratory Medicine, University of Wisconsin-Madison, Madison, Wisconsin 53792, USA

[4]Edison Biotechnology Institute and Heritage College of Osteopathic Medicine, Ohio University, Athens, Ohio 45701, USA

Abstract

Background: Humans with inactivating mutations in *growth hormone receptor (GHR)* have lower rates of cancer, including prostate cancer. Similarly, mice with inactivating *Ghr* mutations are protected from prostatic intraepithelial neoplasia in the C3(1)/TAg prostate cancer model. However, gaps in clinical relevance in those models persist. The current study addresses these gaps and the ongoing role of *Ghr* in prostate cancer using loss-of-function and gain-of-function models.

Methods: Conditional *Ghr* inactivation was achieved in the C3(1)/TAg model by employing a tamoxifen-inducible Cre and a prostate-specific Cre. In parallel, a transgenic GH antagonist was also used. Pathology, proliferation, and gene expression of 6-month old mouse prostates were assessed. Analysis of The Cancer Genome Atlas data was conducted to identify *GHR* overexpression in a subset of human prostate cancers. *Ghr* overexpression was modeled in PTEN-P2 and TRAMP-C2 mouse prostate cancer cells using stable transfectants. The growth, proliferation, and gene expression effects of *Ghr* overexpression was assessed *in vitro* and *in vivo*.

Results: Loss-of-function for *Ghr* globally or in prostatic epithelial cells reduced proliferation and stratification of the prostatic epithelium in the C3(1)/TAg model. Genes and gene sets involved in the immune system and tumorigenesis, for example, were dysregulated upon global *Ghr* disruption. Analysis of The Cancer Genome Atlas revealed higher *GHR* expression in

CORRESPONDANCE: Paul C Marker, PhD (paul.marker@wisc.edu).

AUTHOR CONTRIBUTIONS AND INFORMATION

CJU, SMS, and PCM conceived the animal study and experiment design. CJU, JLP, and AO collected data and carried out experiments. RH assessed tissue pathology. CJU, SJM, and PKT analyzed data. CJU, SJM, and PKT organized and created figures. All authors were involved in writing the paper and had final approval of the submitted and published versions.

DISCLOSURES

The authors have no conflicts of interest to disclose.

human prostate cancers with ERG-fusion genes or ETV1-fusion genes. Modeling the *GHR* overexpression observed in these human prostate cancers by overexpressing *Ghr* in mouse prostate cancer cells with mutant *Pten* or T-antigen driver genes increased proliferation of prostate cancer cells *in vitro* and *in vivo*. *Ghr* overexpression regulated the expression of multiple genes oppositely to *Ghr* loss-of-function models.

Conclusions: Loss-of-function and gain-of-function *Ghr* models, including prostatic epithelial cell specific alterations in *Ghr,* altered proliferation and gene expression. These data suggest that changes in GHR activity in human prostatic epithelial cells play a role in proliferation and gene regulation in prostate cancer, suggesting the potential for disrupting GH signaling, for example by the FDA approved GH antagonist pegvisomant, may be beneficial in treating prostate cancer.

Keywords

GHR; GH; IGF-1; RNA-seq; T-antigen; Pten

INTRODUCTION

Prostate cancer is the most common non-cutaneous cancer affecting men in the United States (1). Common chemotherapeutic agents used to treat a variety of cancers, including prostate cancer, exert a majority of their effects by inducing apoptosis. Insulin-like growth factor 1 (IGF-1) possesses anti-apoptotic properties that can contribute to resistance to chemotherapy (2). However, promising results seen in preclinical lab testing have not shown the same benefit in humans, as blocking IGF-1 signaling alongside other treatments has been shown to have no effect on cancer progression in clinical trials, possibly due to feedback loop mechanisms involving GH that would be hyperactivated upon IGF-1 antagonism (3–6).

Human Laron syndrome is caused by mutations in the growth hormone receptor (GHR) gene that disrupt the GH/IGF-1 axis. Humans and mouse models with GHR mutations possess protections against diseases including cancer—including breast and prostate cancer—and diabetes (7–9). Research focusing on this protection has studied the role of GH and IGF-1 in cancer progression. Higher serum IGF-1 levels correlate with poor prognoses, and although much of the available evidence suggests GH effects in prostate cancer are largely mediated through IGF-1, some effects may be through direct GHR activation in the prostate (10,11). GHR expression has been shown to be differentially regulated in the human prostate cancer cell lines PC3, DU145, and LNCaP depending on their androgen sensitivity (12). The SV40 C3(1) T-antigen (C3(1)/TAg) mouse model of prostate cancer fails to develop PIN lesions when the GH/IGF-1 axis is heritably disrupted, mimicking the cancer protection seen in human Laron patients (9). However, this study fails in modelling the more clinically relevant situation of existing PIN and identifying the therapeutic potential of GH disruption after lesions have formed.

A tamoxifen-inducible Cre was created via the chimeric fusion of Cre to estrogen receptor T2 (Cre-ER^{T2}). Cre-ER^{T2} is normally sequestered in the cytoplasm, however, tamoxifen binding induces a conformational change in the ER (13–15). This binding releases Cre to translocate to the nucleus and freely recombine loxP sites throughout the genome (16,17). When linked to the constitutively active ROSA26 promoter (ROSA βgeo gene trap),

Cre-ER^{T2} becomes a globally inducible, tamoxifen-dependent recombination tool (18,19). The use of tamoxifen inducible Cre to specifically delete functional GHR from mice has been standardized and described elsewhere (20–22). Cre expressed under control of the rat probasin promoter directs expression of Cre to the prostate epithelium in the PbCre4 model (23). The bGH-A122D (GHA) mouse expresses a transgene that creates a competitive antagonist to GH. These mice have lower circulating serum IGF-1 which results in stunted growth early in life (24,25). These three genetic models of GH signaling disruption provided us with the tools to further investigate the role of GH signaling in the C3(1)/TAg transgenic prostate cancer model previously described as developing low-grade PIN at two months, high-grade PIN at five months, and invasive carcinoma at seven months (26).

In this study, we investigated the effects of conditionally deleting *Ghr* in the C3(1)/TAg mouse model of prostate cancer globally and specifically in the prostate epithelium in the C3(1)/TAg model. In both cases, the extent of epithelial stratification and proliferation were reduced suggesting that direct actions of GHR in the prostatic epithelium contribute to these cancer-related phenotypes. Examination of The Cancer Genome Atlas (TCGA) project data (27) also showed increased *GHR* expression in prostate cancers with ERG-fusion genes or ETV1-fusion genes that represent about 50% of prostate cancer cases in man. Modeling this overexpression of *Ghr* increased the growth rate of prostate cancer cells *in vitro* and *in vivo* via increased proliferation and changes in cancer-related gene expression.

MATERIALS AND METHODS

Animal Work Methodology

Mice were housed in polysulfide cages containing corn cob bedding and maintained on a 12-hour light and dark cycle at 20.5 ± 5°C and 30–70% relative humidity. Mice were fed a 5015 Diet (PMI Nutrition International, Brentwood MO) from conception through weaning (post-natal day 21) and an 8604 Teklad Rodent Diet thereafter (Harlan Laboratories, Madison WI). Feed and water were available ad libitum. All procedures were approved by the University of Wisconsin Animal Care and Use Committee and conducted in accordance with the NIH Guide for the Care and Use of Laboratory Animals.

Mice were provided from the Swanson lab from the University of Illinois Chicago and used to establish a breeding colony in our laboratory. C3(1)/TAg mice were maintained on a FVB background while *Ghr*$^{flox/flox}$ (provided by the Kopchick Lab), Rosa-Cre-ER, Probasin-Cre, and GHA (Kopchick Lab) mice were maintained on a C57BL/6J background.

Tamoxifen was compounded to a 75 mg/mL stock concentration in a 5:1 corn oil:ethanol mixture and 250 mg/kg or vehicle control was delivered intraperitoneally for five consecutive days as previously described (20) beginning at 5 months of age. When applicable, mice were sacrificed one month after first dose of tamoxifen or vehicle treatment. Untreated mice were sacrificed at 6 months of age.

Trunk blood was collected at the time of tissue harvest for analysis of serum IGF-1 as described previously (28). Steroid hormone analysis via LC-MS/MS and was adapted from methods previously described (29).

Xenograft surgeries were performed as described previously (28). Briefly, 10-week old Balb/C nu/nu male mice were used as hosts for ~3.5 × 10^5 PTEN-P2 and TRAMP-C2 cells that were transfected with a mouse *Ghr* overexpressing plasmid or an empty vector (EV) control. Cells in collagen were grafted bilaterally under the kidney capsules and harvested after 5 weeks.

RT-qPCR

Complementary DNA (cDNA) was reverse transcribed from RNA extracted from mouse liver and dorsolateral prostate. Gene expression was assessed as an inverse function of cycle threshold (C_t) read by StepOnePlus™ Real-Time PCR System, (4376600; ThermoFisher, Waltham, MA). To determine gene expression relative to the housekeeping gene, TATA Box Binding Protein (TBP), the mean $C_{t,\ TBP}$ was subtracted from the mean $C_{t,\ gene}$. Relative gene copy was two raised to the negative of that difference, like such: $2^{-\left(C_{t,\ gene} - C_{t,\ TBP}\right)}$.

Histology and Immunohistochemistry—Tissues were fixed in 4% paraformaldehyde, dehydrated in alcohol, cleared in Citrisolv, and infiltrated with paraffin. Hematoxylin & eosin (H&E) stains of 5 μm sections of tissue mounted on Superfrost™ Plus Gold Slides (Thermo Fisher Scientific; Waltham, MA) were assessed by a histopathologist.

H&E-stained tissues were assessed blindly according to the following criteria by Dr. Hu, a board-certified pathologist specializing in genitourinary pathology. Epithelial hyperplasia was defined as an increase in epithelial cells within the normal-appearing gland architecture that stand out from the background glands but without cytologic atypia. The increase in epithelial cells was recognized as tufting, nuclear crowding, micropapillary, or even cribriform architecture. PIN was recognized as proliferation of epithelial cells with cytologic atypia such as hyperchromasia, nuclear enlargement, nuclear membrane irregularity or prominent nucleoli within the preexisting glands. PIN was graded as PIN1-PIN4 similarly to previously described (30). Invasive carcinoma was recognized as malignant epithelial proliferation with destructive invasion to stroma.

Cell proliferation was measured via Ki67 immunohistochemistry (IHC) staining as described previously (28).

In Vitro Plasmid Transfection, Selection, and Cell Viability—To create stable transfectants with overexpression of *Ghr* in mouse prostate cancer cells, PTEN-P2 and TRAMP-C2 cells were plated and grown to 70% confluency at which point 1.6 μg of plasmid vector DNA containing mouse *Ghr* (MG50043-UT, Sino biological, Wayne, PA) or pcDNA3.1+ empty vector control was incubated with 4 μg of Lipofectamine 2000 in Transfectgro base media as described by the manufacturer. After 24 hours, cells were split 1:10, incubated for 24 hours, and selected using neomycin for seven days. Transfection and selection was confirmed using qPCR to identify an upregulation in relative *Ghr* expression in cells treated with *Ghr*-expressing plasmids.

Cell viability in culture was assessed using the Promega CellTiter-Blue Cell Viability Assay (G808A; Promega, Madison, WI). Cells were plated at 250 cells/well in 96-well plates 24 hours before the addition of 20 μL of CellTiter-Blue reagent was added to each well and

fluorescence signal was read on a Fluostar Omega fluorescence plate reader (BMG Labtech) at 544/590 nm.

RNA Sequencing

Total RNA submitted to the University of Wisconsin-Madison Biotechnology Center was assayed for purity and integrity and gene expression was assessed as described previously (28). Raw BAM files produced by sequencing can be found at NCBI Gene Expression Omnibus with accession numbers GSE197640 and GSE197683 for WT and C3(1)/TAg prostate RNAseq data, respectively. Bioinformatic analysis of transcriptomic data adhere to recommended ENCODE guidelines and best practices for RNA-Seq and analyzed as described previously (28).

Statistical Analysis

For all histological stains, an ANOVA with Tukey's multiple comparisons test was conducted to identify differences among means. Results are reported as mean ± standard error of the mean (SEM). A difference of $p < 0.05$ was considered significant. All statistics were performed using GraphPad software (GraphPad Software, San Diego, CA).

RESULTS

C3(1)/TAg transgenic mice were bred to mice with a conditionally null allele of *Ghr* in which the 4th exon is flanked by loxP sites (*Ghr*^{flox} mice), mice that ubiquitously express an estrogen-receptor-T2-Cre-recombinase fusion protein from the *Rosa26* locus (Rosa-Cre-ER^{T2} mice), PB-Cre4 transgenic mice that expresses Cre recombinase specifically in prostate epithelial cells (PbCre mice), and/or mice expressing a transgenic GHR antagonist (GHA mice) to generate groups of animals with genotypes *Ghr*$^{flox/flox}$;Rosa-Cre-ER^{T2};C3(1)/TAg$^{+/0}$, *Ghr*$^{flox/flox}$;C3(1)/TAg$^{+/0}$, *Ghr*$^{flox/flox}$;Pb-Cre$^{+/0}$;C3(1)/TAg$^{+/0}$, and GHA$^{+/0}$;C3(1)/TAg$^{+/0}$. Mice with all four of these genotypes had a high incidence of off-target tumors in the head and neck salivary glands resulting in premature death or lethargy requiring euthanasia (Figure 1) that were not described in the original characterization of the C3(1)/TAg model's survivability (26). However, these tumors have previously been identified in a separate study of mammary tumors in this model (31). Due to early mortality, further analysis focused on a 6 month timepoint and five groups of mice with genotype and treatment as follows: *Ghr*$^{flox/flox}$;Rosa-Cre-ER^{T2};C3(1)/TAg$^{+/0}$ with vehicle treatment (vehicle control), *Ghr*$^{flox/flox}$;C3(1)/TAg$^{+/0}$ with tamoxifen treatment (tamoxifen control), *Ghr*$^{flox/flox}$;Rosa-Cre-ER^{T2};C3(1)/TAg$^{+/0}$ with tamoxifen treatment (global *Ghr* deletion), *Ghr*$^{flox/flox}$;Pb-Cre$^{+/0}$;C3(1)/TAg$^{+/0}$ with no treatment (prostate-specific *Ghr* deletion), and GHA$^{+/0}$;C3(1)/TAg$^{+/0}$ with no treatment (GHA). Global *Ghr* deletion in the C3(1)/TAg prostate cancer model reduced *Ghr* RNA expression relative to a housekeeping gene, *Tbp*, in the mouse DLP (Figure 2A) and liver (Figure 2B) and resulted in decreased serum IGF-1 (Figure 2C) and testosterone (Figure 2D) compared to vehicle- and tamoxifen-control tissue and serum. Prostate-specific *Ghr* recombination in the C3(1)/TAg prostate cancer model reduced *Ghr* RNA expression relative to a housekeeping gene, *Tbp*, in the mouse DLP (Figure 2A) but not the liver (Figure 2B) and resulted in no statistically significant change in serum IGF-1 compared to control (Figure 2C). Transgenic GH antagonist expression

in the C3(1)/TAg prostate cancer model induced statistically significant downregulation of *Ghr* in the mouse liver (Figure 2B) but not the DLP (Figure 2A) and resulted in decreased serum IGF-1 compared to control tissue or serum (Figure 2C). There were no statistically significant differences in mouse body weight or prostate wet weight among groups (data not shown).

Histopathological assessment revealed that at 6 months PIN lesions did not develop as extensively in the prostates of C3(1)/TAg mice in our study relative to previous characterization of this model (26). Only one mouse developed identifiable invasive carcinoma in the prostate (tamoxifen control group) while two developed PIN1 (one each in vehicle and tamoxifen control groups). Varying instances of focal tufting without atypia and focal crowding were also observed (Supplementary Table S1). However, extensive epithelial stratification was identified and abundant throughout all groups. All three forms of GH signaling disruption including prostate epithelium specific *Ghr* deletion reduced the extent of prostate epithelial cell stratification in the prostate (Figure 3A–E, K) and reduced epithelial proliferation as determined by Ki67 labeling index (Figure 3F–J, L).

RNA sequencing was performed comparing tamoxifen control DLPs to global *Ghr* deletion DLPs. Blocking GH signaling changed the expression of 75 and 42 genes in C3(1)/TAg and WT DLPs, respectively. Volcano plots of differentially regulated genes' $\log_2$ fold change vs. p-value are shown in Figure 4. Genes with $\log_2$ foldchange greater than 1 are shown in red, and genes with $\log_2$ foldchange less than −1 are shown in cyan. *Ghr* deletion in C3(1)/TAg mice resulted in significant expression changes for 75 genes of which 63 were downregulated (Figure 4A). In WT mice, global *Ghr* deletion significantly changed the expression of 42 genes, 28 of which were downregulated (Figure 4B). Gene set enrichment analysis of canonical gene sets (C2) identified differentially enriched gene sets in C3(1)/TAg and WT mice in Tables 1 and 2, respectively.

Using the UALCAN data portal (32) to interrogate data from the TCGA database (33), we identified statistically significant increases in *GHR* expression relative to normal prostates in prostate cancers with ERG-fusion genes or ETV1-fusion genes that represent about 50% of prostate cancer cases (Figure 5A). On average, there is increased expression of *GHR* in human prostate cancers with ERG-fusions (Figure 5A) as well as a statistically significant positive correlation between GHR expression and ERG expression in prostate tumors (Figure 5B).

Stable transfected derivatives of PTEN-P2 and TRAMP-C2 cell lines were created with expression constructs containing either mouse *Ghr* (PTEN-P2_mGhr and TRAMP-C2_mGhr) or an empty vector control (PTEN-P2_EV and TRAMP-C2_EV). Compared to empty vector controls, the resulting PTEN-P2_mGhr and TRAMP-C2_mGhr overexpressing cells had 2.9- and 2.5-fold increases in mouse *Ghr* expression, respectively (Supplementary Figure S1A). Compared to empty vector controls, PTEN-P2_mGhr and TRAMP-C2_mGhr cells grew faster *in vitro* under standard culture conditions (Supplementary Figure S1B). These four stably transfected cell line derivatives were surgically grafted under the kidney capsules of 10-week-old male Balb/C nu/nu mice for 5 weeks. In both PTEN-P2 and TRAMP-C2 cells, the upregulation of *Ghr* resulted in increased xenograft size and weight

(Figure 6). Similarly, *Ghr* upregulation resulted in increased proliferation as measured by immunohistochemical staining for proliferation marker Ki67 (Figure 7).

RNA was collected from mouse DLPs for *Ghr* deletion and tamoxifen control groups for both C3(1)/TAg and WT background mice. Six genes previously identified to be differentially regulated by GH signaling disruption (28)were found to be down-regulated upon *Ghr* deletion by RNA-seq for both the C3(1)/TAg and WT backgrounds here and were confirmed by quantitative RT-PCR (Figure 8A). RNA was also collected from *Pten* mutant and TRAMP cell line xenografts overexpressing *Ghr* or EV controls. Some of the six genes down-regulated by *Ghr* deletion were regulated in the opposite direction compared to *Ghr* deletion in *Ghr*-overexpressing xenografts with some differences between the *Pten* mutant and TRAMP cell lines (Figure 8B). The expression of four genes previously found to be down-regulated in prostate cancer xenografts by GHR antagonist pegvisomant (*Ccnd1, Ccnd2, Cdk4, and Grem1*) and two genes previously found to be up-regulated in prostate cancer xenografts by pegvisomant (*Ar, Cdh1*) (28) was also evaluated for *Ghr* overexpressing and EV control xenografts and expression of all six genes was oppositely regulated upon *Ghr* overexpression (Figure 8C) compared to the previously observed pattern for pegvisomant-treated xenografts (28).

DISCUSSION

Humans with Laron syndrome appear to be protected from certain diseases, including cancer and diabetes (34). None of the 169 subjects with Laron syndrome in one study developed cancer while their non-Laron relatives developed cancer at expected rates of ~20% (34). Mouse models of Laron syndrome also have lower rates of cancer (35) and are protected from experimentally induced cancer (9). The C3(1)/TAg model of mouse prostate cancer failed to develop PIN as expected when crossed with the mouse model of Laron syndrome (GHR null mice), reflecting an outcome similar to the protection seen in human Laron syndrome subjects (9). However, an important limitation of these epidemiological and experimental studies is that both human Laron patients and the Laron mouse model possess disrupted GH/IGF-1 axes from conception throughout their entire lives, which has limited clinical relevance (21,22). Because of this limitation, these studies fail to address the potential necessity for continuous GH signaling in prostate cancer. To model the potential therapeutic capacity of blocking GH signaling after prostate cancers develop, we used a standardized tamoxifen inducible Cre-lox system (Rosa-Cre-ER) that provided temporal control of *Ghr* expression. Likewise, spatial control of *Ghr* expression (PbCre) provided the opportunity to identify direct action of GH signaling in prostate epithelial cells. Lastly, a transgenically expressed GH antagonist (GHA) gave the ability to mimic chronic GH antagonism and determine its effect on prostate cancer in the C3(1)/TAg model.

GH/IGF-1 axis activity was downregulated in all three models of disruption (Figure 2A–C). Compared to vehicle and tamoxifen control groups, global *Ghr* deletion, prostate-specific *Ghr* deletion, and GHA mice exhibited varying levels of axis disruption. At the RNA level, DLP *Ghr* expression was reduced in both global and prostate-specific deletion groups (Figure 2A). In the liver, *Ghr* RNA was reduced in the global deletion and GHA groups (Figure 2B). GHA-induced downregulation of *Ghr* is consistent with previous investigations

of gene regulation in this model (36). Considering genetic changes, serum IGF-1 was lowered in mice with global *Ghr* and GHA as expected due to blocking GHR function, but not prostate-specific *Ghr* recombination for these mice had an intact axis outside of the prostate epithelium (Figure 2C). Additionally, tamoxifen-induced *Ghr* deletion had reduced serum testosterone (Figure 2D) which is consistent with studies of Laron patients with increased serum testosterone following treatment with IGF-1 (37).

C3(1)/TAg expression transforms cells through mechanisms that are functionally similar to those that occur in human prostate carcinogenesis (26,38). Original characterization of the model identified low-grade PIN in the ventral and dorsolateral lobes of the mouse prostate at two months of age, and high-grade PIN was found in both lobes by five months. Invasive carcinomas were reported in the model as early as seven months. After histopathological assessment by a pathologist, it was revealed that at six months PIN lesions did not develop as extensively in the prostate of C3(1)/TAg mice as originally described. Only one mouse developed identifiable invasive carcinoma in the prostate and two mice displayed instances of PIN1. The lesion penetrance discrepancy between the original characterization and the current study can potentially be due to the mixed background of mice that was required for this study as has been identified in studies of the PTEN mouse prostate cancer model with mixed backgrounds, for example (39). However, extensive epithelial stratification was identified and abundant throughout all groups. Considering these differences in pathology between our model and the original characterization, we found that all three groups with disrupted GH/IGF-1 axes showed reduced prostate duct stratification compared to controls (Figure 3A–E, K). Additionally, proliferation of prostate cells was reduced in GHR-disrupted C3(1)/TAg mice (Figure 3F–J, L).

Decreases in stratification and proliferation in the C3(1)/TAg model were accompanied by changes in gene expression (Figure 4A). C3(1)/TAg prostates in mice with global *Ghr* deletion possessed upregulated gene sets involved in interleukin expression and anti-metastatic genetic mechanisms which hints at GH disruption's contribution to pro-immune, anti-cancer effects (Table 1). These changes in gene expression in the C3(1)/TAg model were mirrored by gene expression changes in the WT mouse DLP, though less robustly (Figure 4B). Differentially enriched gene sets in WT mice with disrupted GH/IGF-1 axes similarly involved the immune system and downregulated genes involved in tumorigenesis, providing further evidence that deletion of *Ghr*, and therefore disruption of the entire GH/IGF1 axis, contributes to transcriptional opposition to carcinogenesis and immune system regulation of uncontrolled growth (Table 2). Given the duplicative representation of the immune system in the current gene and gene set analysis, further examination of the impact of the immune system and immune cell infiltration in the C3(1)/TAg model of cancer is warranted. Additionally, global GHR regulation of immune-related genes in the WT mouse DLP should be explored upstream of the lower urinary tract to determine gene regulation in the prostate. These data align with the translational dysregulation observed in prostate cancer cells treated with pegvisomant in a previous study, indicating that the genetic means of GH disruption outlined here mimic some of the effects of pharmacological GH disruption in terms of downstream transcriptional effects on cancer-related genes and gene sets (28).

Pegvisomant is an FDA-approved GHR antagonist used as a pharmaceutical treatment for acromegaly and has been investigated in models of prostate cancer in combination with enzalutamide resulting in decreased expression of cancerous matrix metalloproteinases and serum prostate specific antigen (40). *In vitro* and pre-clinical *in vivo* studies of pegvisomant's effectiveness in prostate cancer is tantalizing. Previous studies of pegvisomant use *in vitro* and *in vivo* identified therapeutic potential as well as 2,718 differentially expressed genes in *Pten* mutant mouse prostate cancer cells (28). Of these genes, global deletion of *Ghr* similarly changed the expression of seven of them: *Cfb*, *Gcom1*, *Rpl15-ps3*, *Arnt2*, *Cyp4a12a*, *Exph5*, and *Pbk*. The downregulation of *Gcom1*, *Rpl15-ps3*, and *Pbk* infers GH disruption via genetic or pharmacological means has a greater effect on cellular signal transduction than simply blocking the activation of JAK or STAT. Conversely, the upregulation of *Cfb*, *Arnt2*, *Cyp4a12a*, and *Exph5* reinforces gene set analysis that indicates GH disruption plays a role in the upregulation of immune system activity (Tables 1 and 2).

Investigation of differential expression of genes in C3(1)/TAg and WT mice identify a few genes of interest that are regulated in part by AR. Interestingly, while one study observed a tamoxifen-induced increase in testosterone levels in acromegaly patients (41), tamoxifen-induced deletion of *Ghr* resulted in decreased serum testosterone (Figure 2D). Conversely, another study observed an increase in testosterone in Laron patients supplemented with IGF-1 (37). These findings suggest that GH may have an indirect role in promoting androgen-regulated genes in prostate cancer.

Previous studies have identified that local expression and overexpression of GH occurs in advanced human prostate cancers and contributes to cancer progression (40). This study identified GHR as an additional component of the GH signaling pathway that is altered in prostate cancer. UALCAN data portal interrogation of TCGA data revealed an overexpression of GHR relative to normal prostate in human prostate cancers with ERG-fusion genes or ETV1-fusion genes (Figure 5A). These two subtypes represent about half of all prostate cancer cases (33). Additionally, a positive correlation links GHR and ERG expression in human prostate tumors (Figure 5B). We speculate that pathways downstream of GHR may be playing a cooperative role with ETS fusion genes which has similarly been reported in PI3K pathway activation (42). To further highlight this relationship between GHR and prostate tumors, we found that PTEN-P2 and TRAMP-C2 mouse prostate cancer cells that overexpress mouse *Ghr* grew more robustly than normal *Ghr* controls (Figure 6). Similarly, both PTEN-P2 and TRAMP-C2 *Ghr* overexpressing cells had a higher proliferation rate when grown *in vivo* than controls (Figure 7). PTEN-P2 cells' transformation is driven by a heterozygous deletion of the tumor suppressor gene *Pten* while TRAMP-C2 is derived from a similar C3(1)/TAg-induced carcinoma used in genetic studies here (43,44). These data reveal a cooperation between *Ghr* overexpression and multiple oncogenic insults to drive tumor growth. While previous studies have identified the cancer driving potential of autocrine GH signaling (45), this study provides the first functional evidence that *Ghr* overexpression may drive prostate cancer progression. Additionally, overexpression of *Ghr* resulted in the opposite regulation of genes previously implicated in this study via tamoxifen-induced *Ghr* deletion (Figure 4) or with pegvisomant treatment ((28); Figure 8). For example, all commonly differentially regulated genes in C3(1)/TAg and

WT mouse prostates were downregulated after *Ghr* deletion. *Ghr* overexpression, however, induced upregulation of some of those genes (Figure 8B). As well, pegvisomant treatment altered gene expression in PTEN-P2 and TRAMP-C2 cells in the opposite manner that *Ghr* overexpression did here ((28); Figure 8C). These data describing the overexpression of GHR in human prostate cancers with ERG- and ETV1-fusion genes provides rationale to develop a new transgenic model with prostate-specific *Ghr* overexpression. This model would provide a way to investigate the potential role of *Ghr* as a driver of prostate cancer initiation and progression and the relationship between the GH/IGF-1 axis and fusion genes involving the ETS family of transcription factors.

CONCLUSIONS

In this study, we investigated the effects of conditionally deleting *Ghr* in the C3(1)/TAg mouse model of prostate cancer. This study showed that GH/IGF-1 axis disruption through global *Ghr* deletion, prostate-specific *Ghr* deletion, or GHA expression reduced the extent of prostate epithelial stratification in the C3(1)/TAg model through decreased proliferation. By deleting *Ghr* specifically in the prostate epithelium, we've shown that GHR activity directly contributes to cellular transformation and proliferation. Further, gene regulation downstream of GHR and IGF-1 was significantly altered upon global deletion of *Ghr*. Overexpression of *Ghr* also increased tumor size of xenografted mouse prostate cancer cells. Together, these loss-of-function and gain-of-function models that altered GHR activity demonstrated a pro-proliferative role for GHR in prostate cancer cells and point to a potentially clinically relevant target for prostate cancer treatment.

Supplementary Material

Refer to Web version on PubMed Central for supplementary material.

ACKNOWLEDGEMENTS

This work was supported by the National Cancer Institute (R21CA238105). The content of this work is solely the responsibility of the authors and does not necessarily represent the official views of the National Cancer Institute. Special thanks to Sandra Splinter BonDurant and Molly Zeller at the University of Wisconsin-Madison Biotechnology Center DNA Sequencing Facility and Amita Kapoor and Cody Corbett at the Wisconsin National Primate Research Center.

DATA AVAILABILITY

RNA-Seq data is available for download from NCBI Gene Expression Omnibus (https://www.ncbi.nlm.nih.gov/GEO) with accession numbers GSE197640 and GSE197683. Additional data are available from the corresponding author upon reasonable request.

REFERENCES

1. Ferlay J, Soerjomataram I, Dikshit R, Eser S, Mathers C, Rebelo M, Parkin DM, Forman D, Bray F. Cancer incidence and mortality worldwide: sources, methods and major patterns in GLOBOCAN 2012. Int J Cancer. 2015;136(5):E359–386. [PubMed: 25220842]
2. Jan R, Chaudhry GE. Understanding Apoptosis and Apoptotic Pathways Targeted Cancer Therapeutics. Adv Pharm Bull. 2019;9(2):205–218. [PubMed: 31380246]

3. Data from: A Study to Evaluate the Biological Activity of R1507 in Women With Operable Breast Cancer. Identifier NCT00882674 July 2009-December 2010. https://ClinicalTrials.gov/show/NCT00882674.

4. Data from: A Multiple Ascending Dose Study of R1507 in Children and Adolescents With Advanced Solid Tumors. Identifier NCT00560144 December 2007-December 2011. https://ClinicalTrials.gov/show/NCT00560144.

5. Data from: A Study of R1507 in Combination With Multiple Standard Chemotherapy Treatments in Patients With Advanced Solid Tumors. Identifier NCT00811993 February 2009-December 2012. https://ClinicalTrials.gov/show/NCT00811993.

6. Data from: A Study of R1507 in Combination With Letrozole in Postmenopausal Women With Advanced Breast Cancer. Identifier NCT00796107 January 2009-March 2010.

7. Janecka A, Kołodziej-Rzepa M, Biesaga B. Clinical and Molecular Features of Laron Syndrome, A Genetic Disorder Protecting from Cancer. In Vivo. 2016;30(4):375–381. [PubMed: 27381597]

8. Steuerman R, Shevah O, Laron Z. Congenital IGF1 deficiency tends to confer protection against post-natal development of malignancies. Eur J Endocrinol. 2011;164(4):485–489. [PubMed: 21292919]

9. Wang Z, Prins GS, Coschigano KT, Kopchick JJ, Green JE, Ray VH, Hedayat S, Christov KT, Unterman TG, Swanson SM. Disruption of growth hormone signaling retards early stages of prostate carcinogenesis in the C3(1)/T antigen mouse. Endocrinology. 2005;146(12):5188–5196. [PubMed: 16141391]

10. Travis RC, Appleby PN, Martin RM, Holly JMP, Albanes D, Black A, Bueno-de-Mesquita HBA, Chan JM, Chen C, Chirlaque MD, Cook MB, Deschasaux M, Donovan JL, Ferrucci L, Galan P, Giles GG, Giovannucci EL, Gunter MJ, Habel LA, Hamdy FC, Helzlsouer KJ, Hercberg S, Hoover RN, Janssen J, Kaaks R, Kubo T, Le Marchand L, Metter EJ, Mikami K, Morris JK, Neal DE, Neuhouser ML, Ozasa K, Palli D, Platz EA, Pollak M, Price AJ, Roobol MJ, Schaefer C, Schenk JM, Severi G, Stampfer MJ, Stattin P, Tamakoshi A, Tangen CM, Touvier M, Wald NJ, Weiss NS, Ziegler RG, Key TJ, Allen NE. A Meta-analysis of Individual Participant Data Reveals an Association between Circulating Levels of IGF-I and Prostate Cancer Risk. Cancer Res. 2016;76(8):2288–2300. [PubMed: 26921328]

11. Watts EL, Fensom GK, Smith Byrne K, Perez-Cornago A, Allen NE, Knuppel A, Gunter MJ, Holmes MV, Martin RM, Murphy N, Tsilidis KK, Yeap BB, Key TJ, Travis RC. Circulating insulin-like growth factor-I, total and free testosterone concentrations and prostate cancer risk in 200 000 men in UK Biobank. Int J Cancer. 2021;148(9):2274–2288. [PubMed: 33252839]

12. Bidosee M, Karry R, Weiss-Messer E, Barkey RJ. Regulation of growth hormone receptors in human prostate cancer cell lines. Mol Cell Endocrinol. 2009;309(1–2):82–92. [PubMed: 19540305]

13. Borgna JaHR. Hydroxylated Metabolites of Tamoxifen Are Formed in Vivo and Bound to Estrogen Receptor in Target Tissues. The Journal of Biological Chemistry. 1981;256(2):8550–8868.

14. Jordan V, Collins M, Rowsby L, and Prestwich G. A monohydroxylated metabolite of tamoxifen with potent antioestrogenic activity. Journal of Endocrinology. 1977;75(2):305–316. [PubMed: 591813]

15. Robertson D, Katzenellenbogen J, Long D, Rorke E, and Katzenellenbogen B. Tamoxifen antiestrogens. A comparison of the activity, pharmacokinetics, and metabolic activation of the *cis* and *trans* isomers of tamoxifen. Journal of Steroid Biochemistry. 1982;16:1–13. [PubMed: 7062732]

16. Feil R, Wagner J, Metzger D, and Chambon P. Regulation of cre recombinase activity by mutated estrogen receptor ligand-binding domains. Biochemical and Biophyscial Research Communications. 1997;237:752–757.

17. Indra A, Warot X, Brocard J, Bornert J, Xiao J, Chambon P, and Metzger D. Temporally-controlled site-specific mutagensis in the basal layer of the epidermis: comparison of the recombinase activity of the tamoxifen-inducible Cre-ER^{T} and Cre-ER^{T2} recombinases. Nucleic Acids Research. 1999;27(22):4324–4327. [PubMed: 10536138]

18. Ventura A, Kirsch DG, McLaughlin ME, Tuveson DA, Grimm J, Lintault L, Newman J, Reczek EE, Weissleder R, Jacks T. Restoration of p53 function leads to tumour regression in vivo. Nature. 2007;445(7128):661–665. [PubMed: 17251932]

19. Zambrowicz B, Imamoto A, Fiering S, Herzenberg L, Kerr W, and Soriano P. Disruption of overlapping transcripts in the ROSA βetageo 26 gene trap strain leads to widespread expression of b-galactosidase in mouse embryos and hematopoietic cells. Developmental Biology. 1997;94:3789–3794.

20. Duran-Ortiz S, Bell S, Kopchick JJ. Standardizing protocols dealing with growth hormone receptor gene disruption in mice using the Cre-lox system. Growth Horm IGF Res. 2018;42–43:52–57.

21. Junnila RK, List EO, Berryman DE, Murrey JW, Kopchick JJ. The GH/IGF-1 axis in ageing and longevity. Nature reviews Endocrinology. 2013;9(6):366–376.

22. Duran-Ortiz S, List EO, Ikeno Y, Young J, Basu R, Bell S, McHugh T, Funk K, Mathes S, Qian Y, Kulkarni P, Yakar S, Berryman DE, Kopchick JJ. Growth hormone receptor gene disruption in mature-adult mice improves male insulin sensitivity and extends female lifespan. Aging cell. 2021;20(12):e13506. [PubMed: 34811874]

23. Wu X, Wu J, Huang J, Powell W, Zhang J, Matusik R, Sangiorgi F, Maxson R, Sucov H, and Roy-Burman P. Generation of a prostate epithelial cell-specifc Cre transgenic mouse model for tissue-specifc gene ablation. Mechanisms of Development. 2001;101:61–69. [PubMed: 11231059]

24. Coschigano KT, Holland AN, Riders ME, List EO, Flyvbjerg A, Kopchick JJ. Deletion, but not antagonism, of the mouse growth hormone receptor results in severely decreased body weights, insulin, and insulin-like growth factor I levels and increased life span. Endocrinology. 2003;144(9):3799–3810. [PubMed: 12933651]

25. Chen W, Wright D, Mehta B, Wagner T, and Kopchick J. Expression of a mutated bovine growth hormone gene suppresses growth of transgenic mice. Cell Biology. 1990;87:5061–5065.

26. Shibata M, Ward JM, Devor DE, Liu M, and Green JE. Progression of Prostatic Intraepithelial Neoplasia to Invasive Carcinoma in C3(1)/SV4O Large T Antigen Transgenic Mice: Histopathological and Molecular Biological Alterations'. Cancer Research. 1996;56:4894–4903. [PubMed: 8895741]

27. Institute NC. The Cancer Genome Atlas (TCGA) Research Network.

28. Unterberger CJ, Maklakova VI, Lazar M, Arneson PD, Mcilwain SJ, Tsourkas PK, Hu R, Kopchick JJ, Swanson SSM, and Marker PC. GH action in prostate cancer cells promotes proliferation limits apoptosis and regulates cancer-related gene expression. Endocrinology. 2022;163(5).

29. Kenealy BP, Kapoor A, Guerriero KA, Keen KL, Garcia JP, Kurian JR, Ziegler TE, Terasawa E. Neuroestradiol in the Hypothalamus Contributes to the Regulation of Gonadotropin Releasing Hormone Release. The Journal of Neuroscience. 2013;33(49):19051–19059. [PubMed: 24305803]

30. Park JH, Walls JE, Galvez JJ, Kim M, Abate-Shen C, Shen MM, Cardiff RD. Prostatic intraepithelial neoplasia in genetically engineered mice. The American journal of pathology. 2002;161(2):727–735. [PubMed: 12163397]

31. Shibata M-A, Jorcyk CL, Liu M-L, Yoshidome K, Gold LG, Green JE. The C3(1)/SV40 T Antigen Transgenic Mouse Model of Prostate and Mammary Cancer. Toxicologic pathology. 1998;26(1):177–182. [PubMed: 9502400]

32. Chandrashekar DS, Bashel B, Balasubramanya SAH, Creighton CJ, Ponce-Rodriguez I, Chakravarthi B, Varambally S. UALCAN: A Portal for Facilitating Tumor Subgroup Gene Expression and Survival Analyses. Neoplasia. 2017;19(8):649–658. [PubMed: 28732212]

33. The Molecular Taxonomy of Primary Prostate Cancer. Cell. 2015;163(4):1011–1025. [PubMed: 26544944]

34. Guevara-Aguirre J, Balasubramanian P, Guevara-Aguirre M, Wei M, Madia F, Cheng CW, Hwang D, Martin-Montalvo A, Saavedra J, Ingles S, de Cabo R, Cohen P, Longo VD. Growth hormone receptor deficiency is associated with a major reduction in pro-aging signaling, cancer, and diabetes in humans. Sci Transl Med. 2011;3(70):70ra13.

35. Ikeno Y, Hubbard GB, Lee S, Cortez LA, Lew CM, Webb CR, Berryman DE, List EO, Kopchick JJ, Bartke A. Reduced incidence and delayed occurrence of fatal neoplastic diseases in growth hormone receptor/binding protein knockout mice. The journals of gerontology Series A, Biological sciences and medical sciences. 2009;64(5):522–529. [PubMed: 19228785]

36. Iida K, Del Rincon JP, Kim D-S, Itoh E, Nass R, Coschigano KT, Kopchick JJ, Thorner MO. Tissue-Specific Regulation of Growth Hormone (GH) Receptor and Insulin-Like Growth Factor-I

Gene Expression in the Pituitary and Liver of GH-Deficient (lit/lit) Mice and Transgenic Mice that Overexpress Bovine GH (bGH) or a bGH Antagonist. Endocrinology. 2004;145(4):1564–1570. [PubMed: 14726438]

37. Laron Z, Klinger B. Effect of insulin-like growth factor-I treatment on serum androgens and testicular and penile size in males with Laron syndrome (primary growth hormone resistance). Eur J Endocrinol. 1998;138(2):176–180. [PubMed: 9506862]
38. Bostwick DG. High grade prostatic intraepithelial neoplasia. The most likely precursor of prostate cancer. Cancer. 1995;75(S7):1823–1836.
39. Wang S, Gao J, Lei Q, Rozengurt N, Pritchard C, Jiao J, Thomas GV, Li G, Roy-Burman P, Nelson PS, Liu X, Wu H. Prostate-specific deletion of the murine Pten tumor suppressor gene leads to metastatic prostate cancer. Cancer Cell. 2003;4(3):209–221. [PubMed: 14522255]
40. Recouvreux MV, Wu JB, Gao AC, Zonis S, Chesnokova V, Bhowmick N, Chung LW, Melmed S. Androgen Receptor Regulation of Local Growth Hormone in Prostate Cancer Cells. Endocrinology. 2017;158(7):2255–2268. [PubMed: 28444169]
41. Balili I, Barkan A. Tamoxifen as a therapeutic agent in acromegaly. Pituitary. 2014;17(6):500–504. [PubMed: 24243064]
42. Carver BS, Tran J, Gopalan A, Chen Z, Shaikh S, Carracedo A, Alimonti A, Nardella C, Varmeh S, Scardino PT, Cordon-Cardo C, Gerald W, Pandolfi PP. Aberrant ERG expression cooperates with loss of PTEN to promote cancer progression in the prostate. Nature genetics. 2009;41(5):619–624. [PubMed: 19396168]
43. Foster BA, Gingrich JR, Kwon ED, Madias C, Greenberg NM. Characterization of prostatic epithelial cell lines derived from transgenic adenocarcinoma of the mouse prostate (TRAMP) model. Cancer Res. 1997;57(16):3325–3330. [PubMed: 9269988]
44. Jiao J, Wang S, Qiao R, Vivanco I, Watson PA, Sawyers CL, Wu H. Murine Cell Lines Derived from Pten Null Prostate Cancer Show the Critical Role of PTEN in Hormone Refractory Prostate Cancer Development. Cancer Research. 2007;67(13):6083–6091. [PubMed: 17616663]
45. Mukhina S, Mertani HC, Guo K, Lee K-O, Gluckman PD, Lobie PE. Phenotypic conversion of human mammary carcinoma cells by autocrine human growth hormone. Proceedings of the National Academy of Sciences. 2004;101(42):15166–15171.

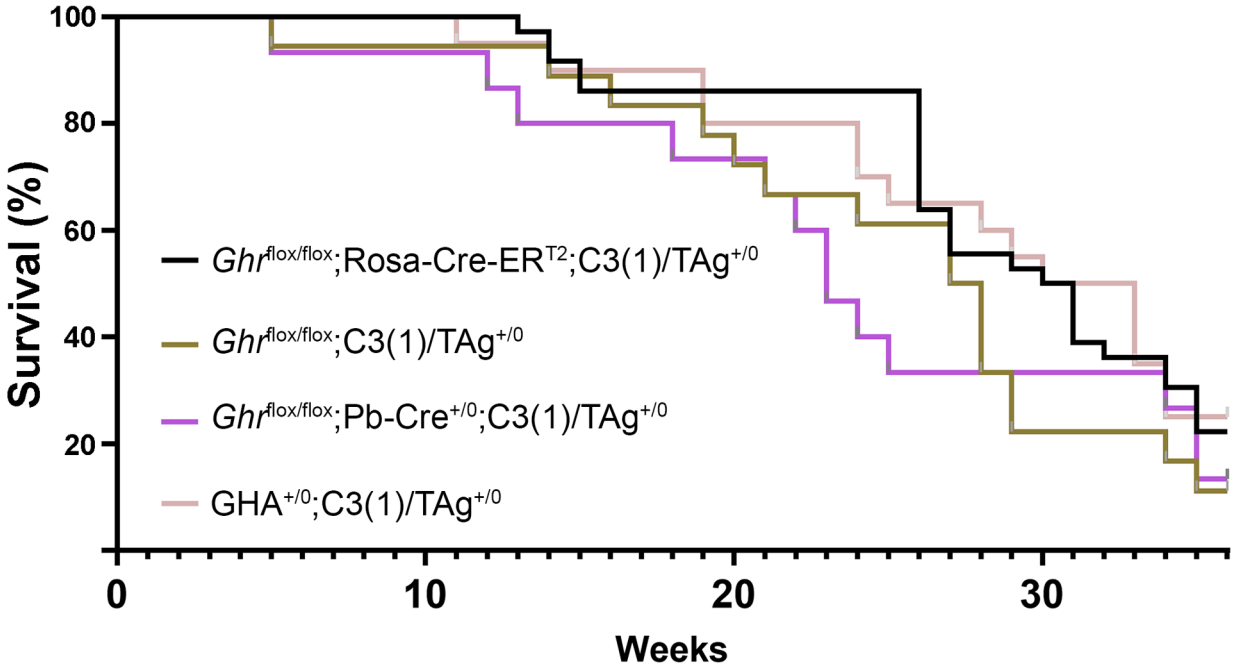

Figure 1.

A Kaplan-Meier curve is shown for genotypes *Ghr*$^{flox/flox}$;Rosa-Cre-ER^{T2};C3(1)/TAg$^{+/0}$ (n=36), *Ghr*$^{flox/flox}$;C3(1)/TAg$^{+/0}$ (n=18), *Ghr*$^{flox/flox}$;Pb-Cre$^{+/0}$;C3(1)/TAg$^{+/0}$ (n=15), and GHA$^{+/0}$;C3(1)/TAg$^{+/0}$ (n=20). A Mantel-Cox log-rank text reveals no significant difference in survival curves between groups.

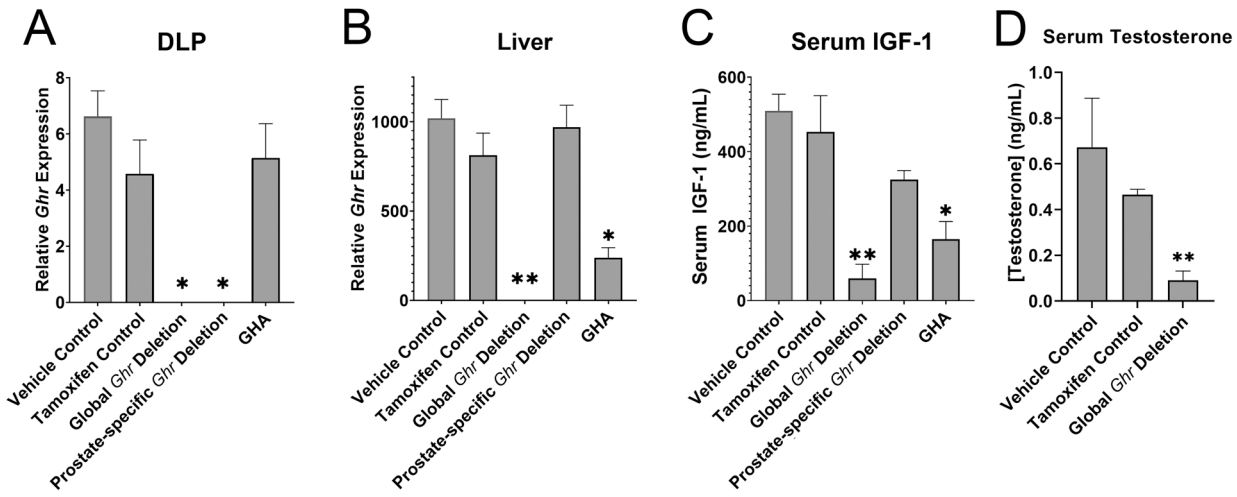

Figure 2.

RT-qPCR was used to measure *Ghr* expression in the DLP **(A)** and livers **(B)** of mice. Expression is presented relative to the expression of the housekeeping gene *Tbp*. Serum IGF-1 levels were measured by ELISA **(C)**. Serum testosterone was quantified by LC-MS/MS **(D)**. N = 3–7 per group. Statistically significant differences from vehicle control determined by ANOVA with Tukey's multiple comparison's test are indicated; *p<0.05, **p<0.01.

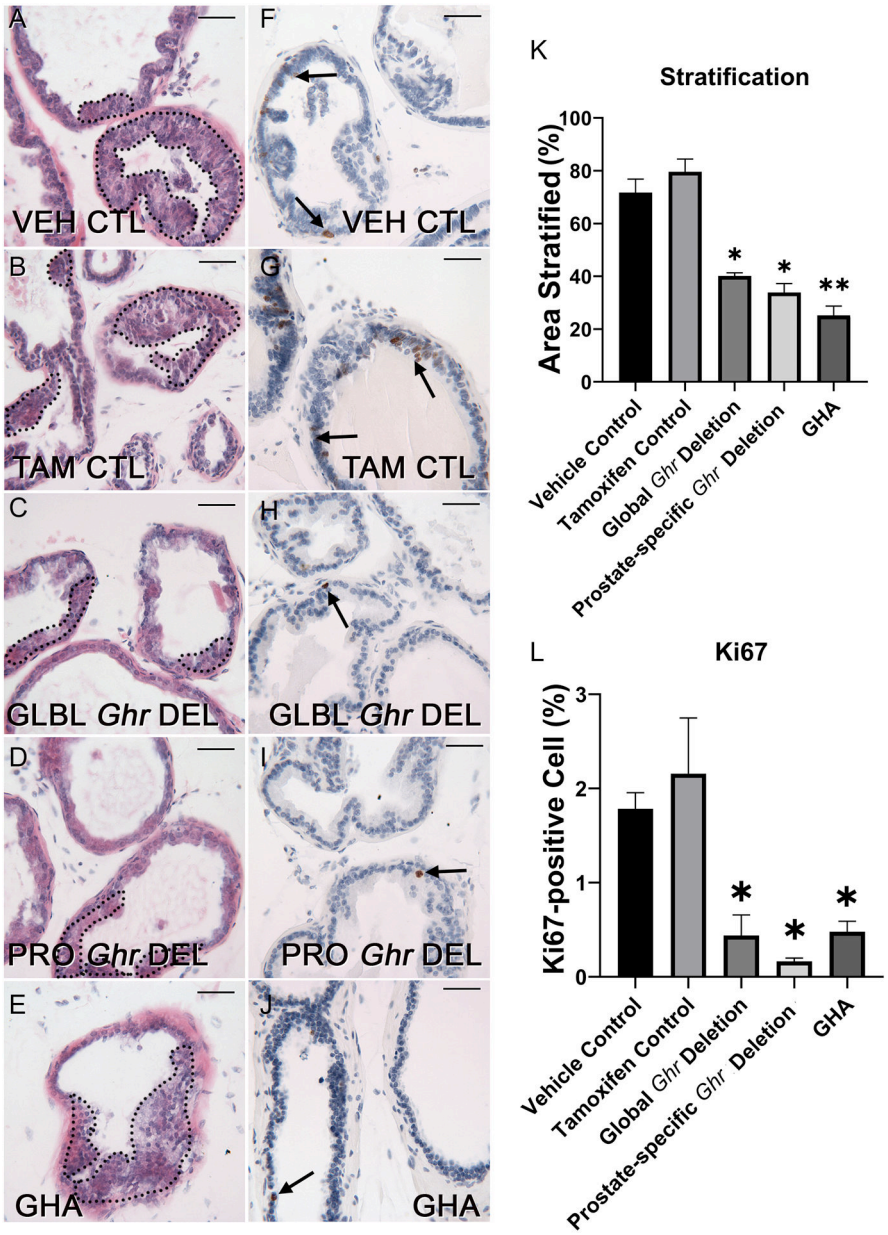

Figure 3.

Representative images of H&E-stained **(A-E)** and Ki67-stained **(F-J)** sections are shown for vehicle control **(A, F)**, tamoxifen control **(B, G)**, global *Ghr* deletion **(C, H)** prostate-specific *Ghr* deletion **(D, I)** and GHA **(E, J)** mouse DLPs. Scale bar for each image = 50 μm. Dotted borders in **A-E** highlight examples of areas identified as epithelial stratification for quantification purposes. Arrows in **F-J** point to examples of Ki67 positive cells (brown stain). **(K)** Area of stratification was assessed by an observer blinded to group and taken as a percentage of total prostatic area with a multi-layered epithelium (n=3–6 per group). **(L)** Ki67 labeling index was determined by counting Ki67 positive cells and total cells based in nuclear hematoxylin stain by an observer blinded to group, (n=3–5 per group). Statistically

significant differences determined by ANOVA and Tukey's multiple comparisons test are indicated, *$p<0.05$, **$p<0.01$.

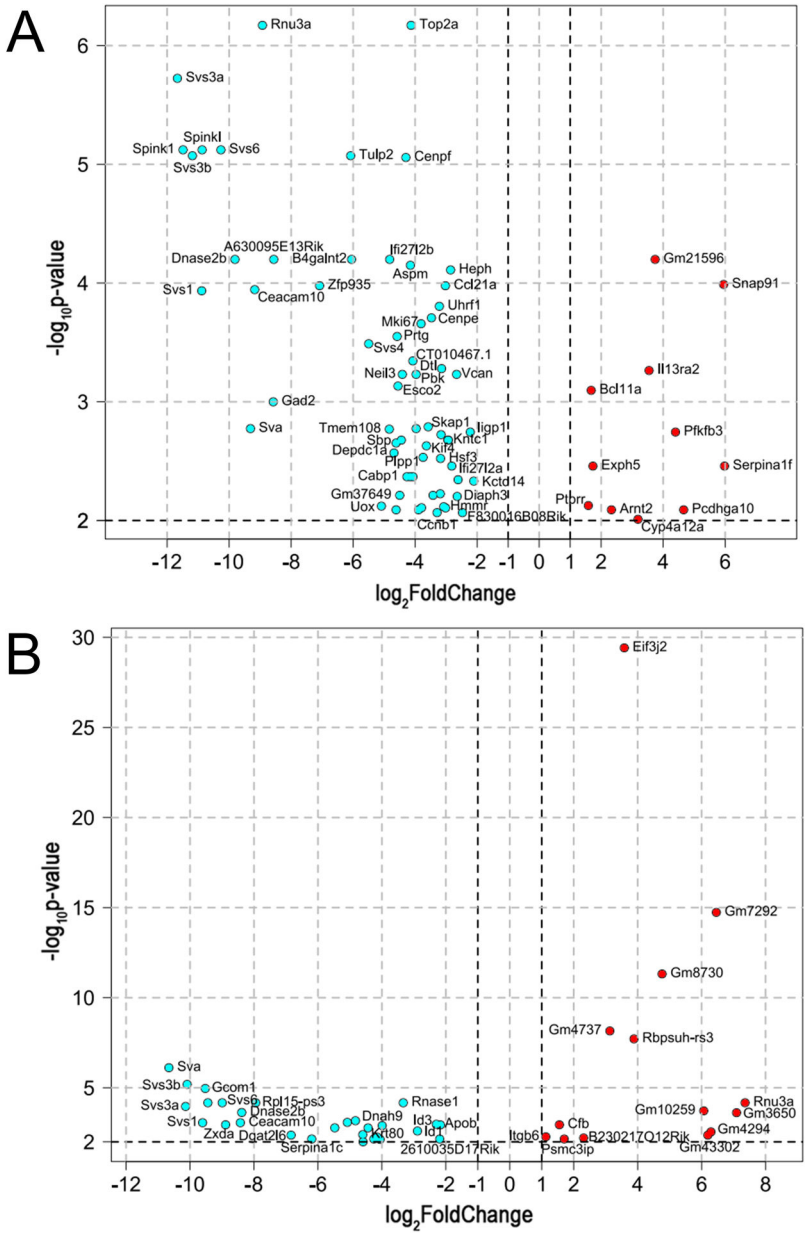

Figure 4.

A volcano plot of differentially expressed genes in the DLP of C3(1)/TAg **(A)** and WT **(B)** mice with tamoxifen-induced *Ghr* deletion compared tamoxifen treated controls with $\log_2$ fold change on the x-axis and the negative $\log_{10}$ of the adjusted p-value on the y-axis. Thresholds for significance are $-\log_{10}$p-value > 2 and $\log_2$FoldChange > 1 or < −1. Genes upregulated in response to *Ghr* deletion are colored red, and genes downregulated in response to *Ghr* deletion are colored cyan.

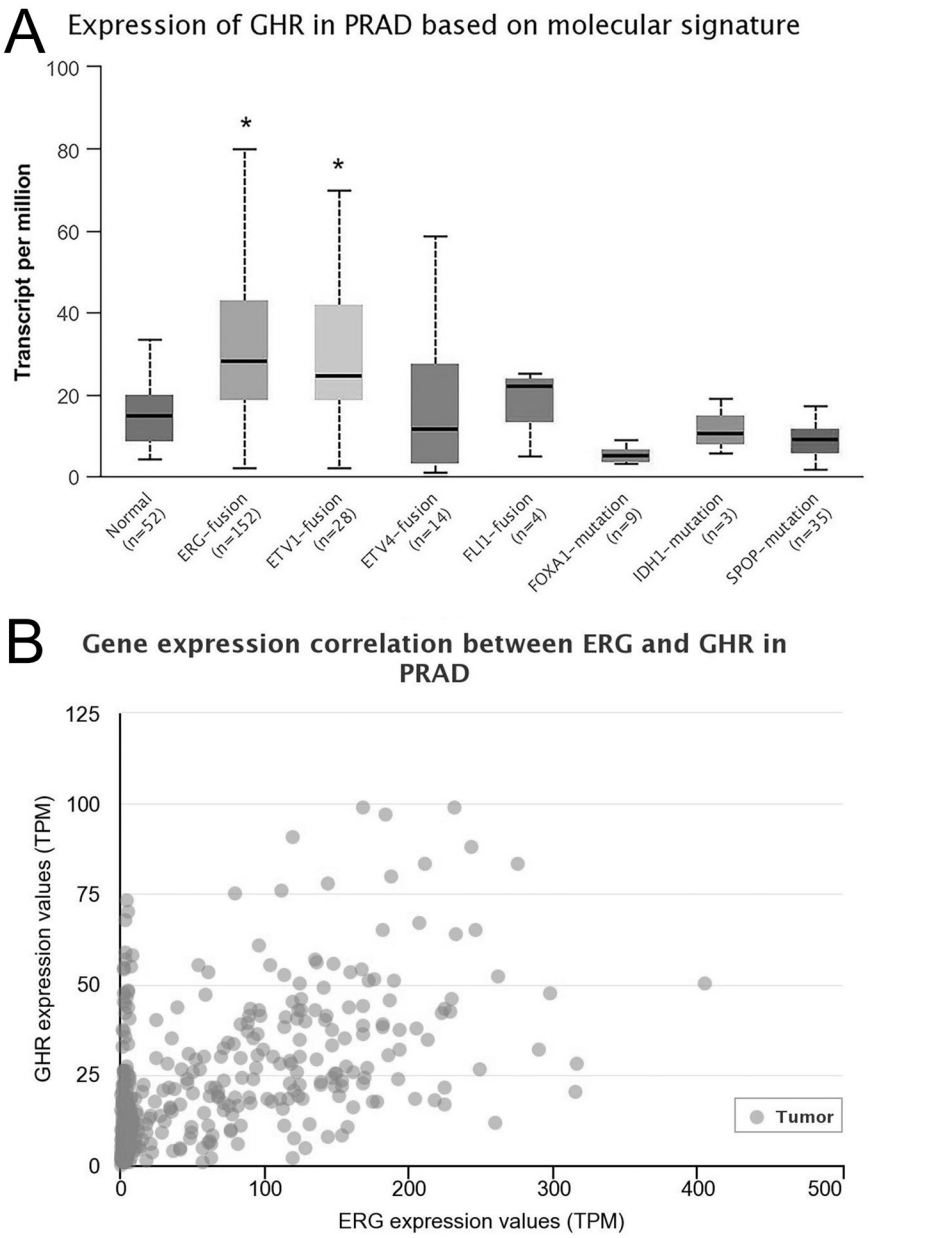

Figure 5.

TCGA project data for *GHR* expression in human prostate cancers separated by molecular signature are shown (A) (data visualization and statistics via the UALCAN data portal, $p<1\times10^{-12}$ for normal vs ERG-fusion, $p=1.16\times10^{-4}$ for normal vs ETV1-fusion). The UALCAN data portal was used to compare *GHR* (vertical axis) and *ERG* (horizontal axis) expression in TCGA prostate tumors **(B).** Pearson Correlation coefficient: 0.58.

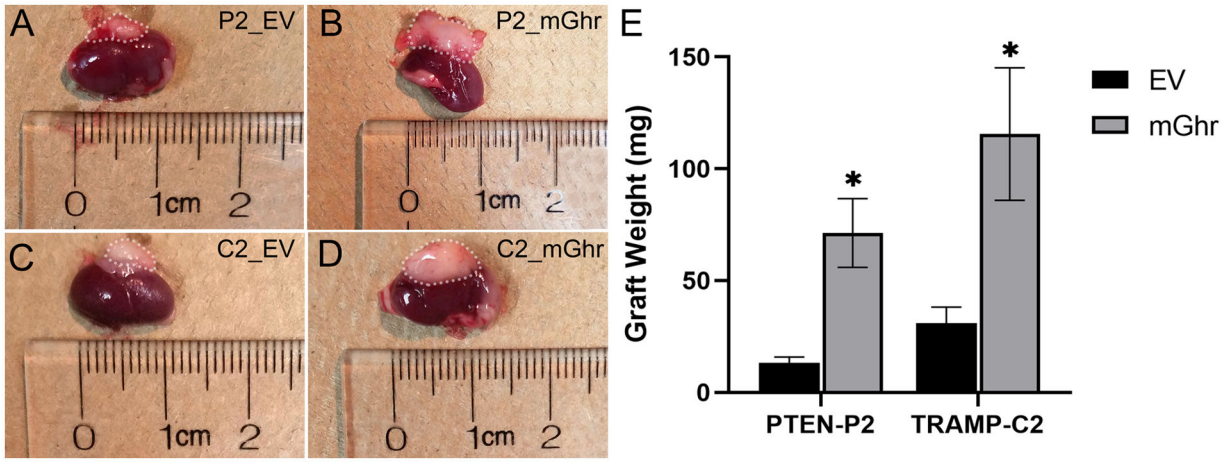

Figure 6.

PTEN-P2 or TRAMP-C2 cells stably transfected with a plasmid containing either mouse *Ghr* (_mGhr) or an empty vector control (_EV) suspended in rat collagen pellets (3.5×10^5 cells per graft) were surgically grafted under the kidney capsules of 10-week-old male Balb/C nu/nu mice. Xenografts were grown for 5 weeks. Examples of resultant xenografts are shown for PTEN-P2_EV **(A)**, PTEN-P2_mGhr **(B)**, TRAMP-C2_EV **(C)** and TRAMP-C2_mGhr **(D)**. Photos in A-D show kidneys (dark red) with xenografts (lighter areas on kidney surface inside the dashed lines) and a ruler for scale. **(E)** Graft masses are shown for empty vector controls (black bars, n=5 per group) and *Ghr* upregulated (grey bars, n=4 per group). Statistically significant differences from control are indicated *$p<0.05$; Student's t-test).

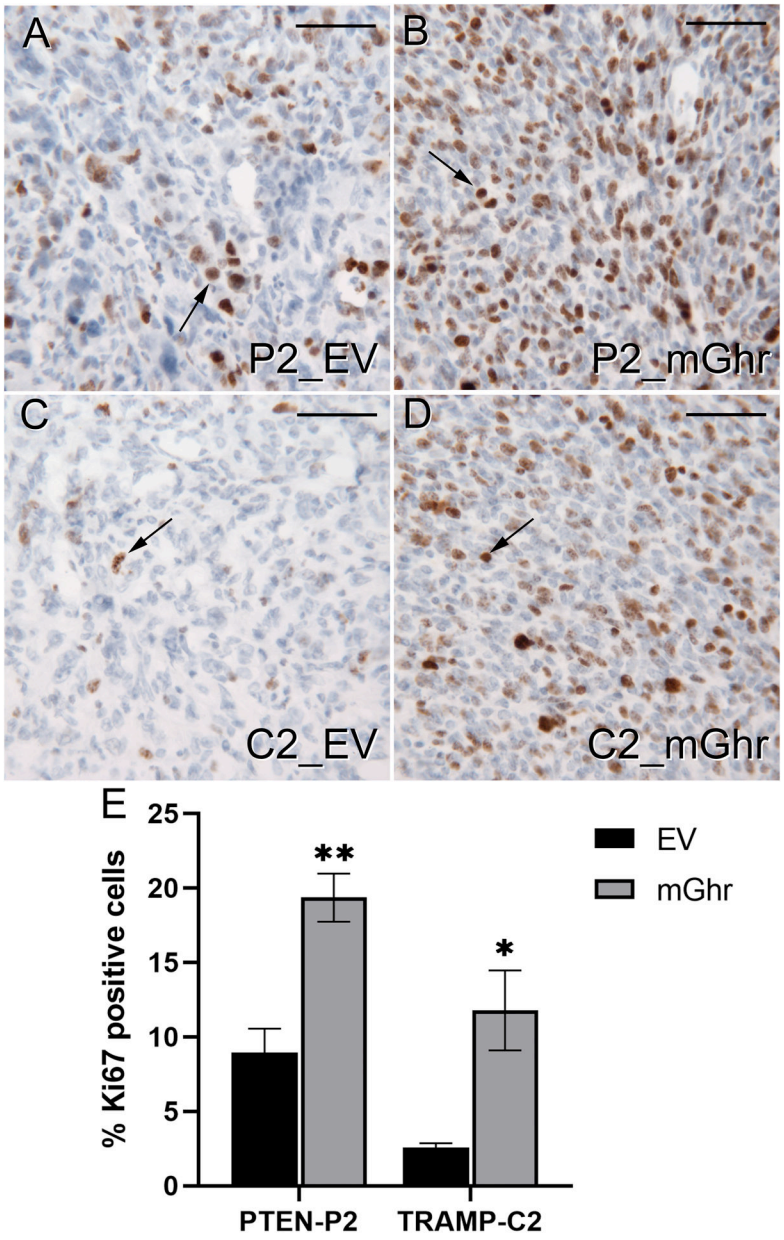

Figure 7.

Representative images of Ki67-stained sections are shown for PTEN-P2_EV **(A)**, PTEN-P2_mGhr **(B)**, TRAMP-C2_EV **(C)** and TRAMP-C2_mGhr **(D)**. Scale bar for each image = 50 μm. Arrows point to examples of Ki67 positive cells (brown stain). **(E)** Ki67 labeling index was determined by counting Ki67 positive cells and total cells based in nuclear hematoxylin stain by an observer blinded to group, n=4 per group. Statistically significant differences determined by ANOVA are indicated, *p<0.05, **p<0.01.

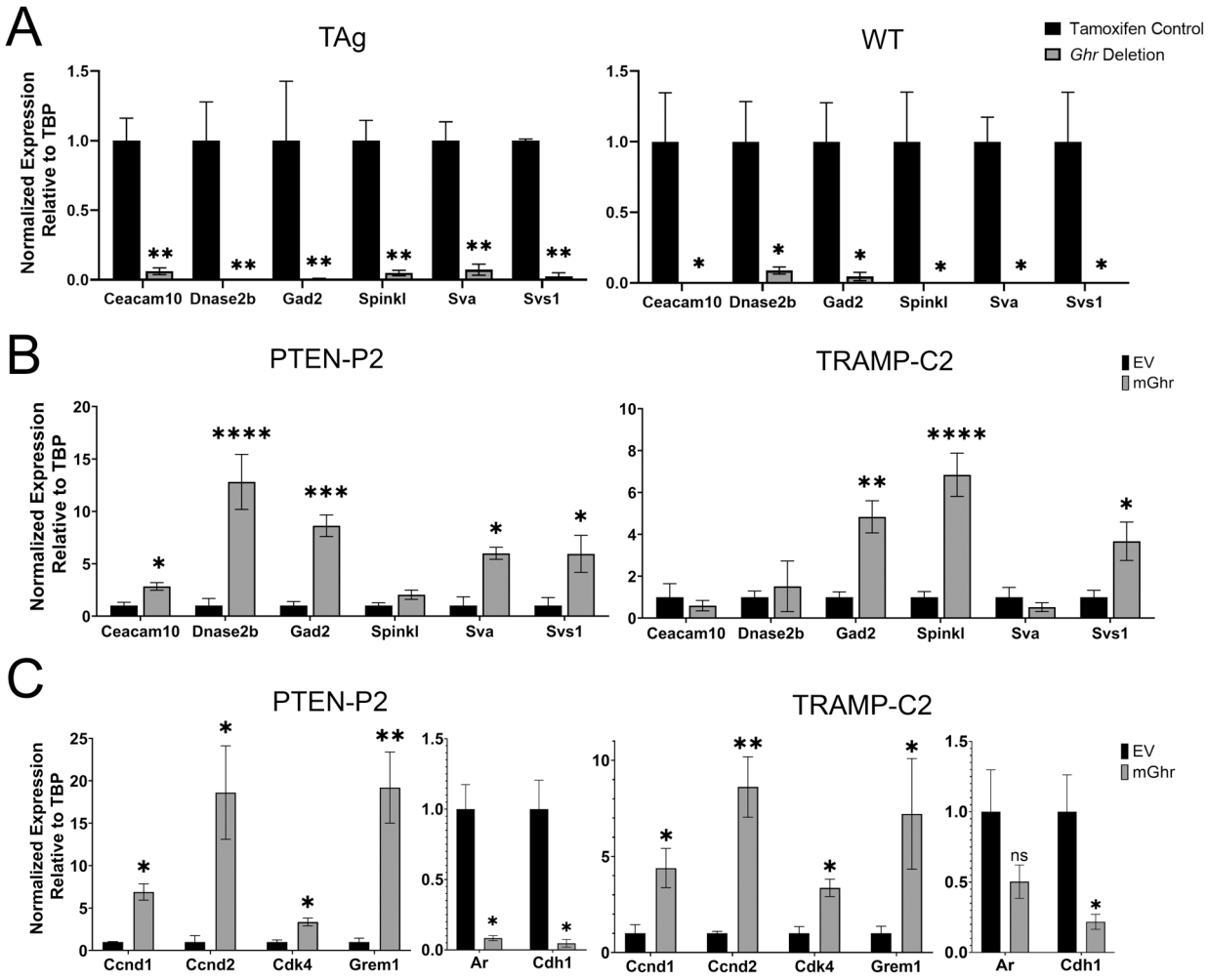

Figure 8.

RNA extracted from DLPs of global *Ghr* deletion or tamoxifen groups in C3(1)/TAg and WT mice were used to confirm expression changes via RT-qPCR in genes first identified by RNA-seq **(A)**. Gene expression as measured by qPCR in PTEN-P2 and TRAMP-C2 grafts with overexpression of *Ghr* (mGhr) compared to empty vector (EV) controls for genes identified as *Ghr* regulated in this study **(B)** and genes previously implicated by disruption of the GH/IGF-1 axis with pegvisomant treatment (28) **(C).** Gene expression is shown relative to the expression of the housekeeping gene, *Tbp*, and normalized to control = 1. Statistically significant differences determined by ANOVA with Tukey's multiple comparison's test are indicated, *p<0.05, **p<0.01; n = 3–4 per group.

Table 1.

Differentially enriched C2 genesin C3(1)/TAg mouse DLPs upon *Ghr* deletion.

Gene Set name	log_2FoldChange	Corrected p-value
REACTOME_INTERLEUKIN_1_FAMILY_SIGNALING	1.7413	2.914×10^{-6}
KRIGE_RESPONSE_TO_TOSEDOSTAT_24HR_DN	1.7289	3.384×10^{-6}
THUM_SYSTOLIC_HEART_FAILURE_DN	1.7121	4.073×10^{-6}
LOCKWOOD_AMPLIFIED_IN_LUNG_CANCER	1.7090	4.318×10^{-6}
GRESHOCK_CANCER_COPY_NUMBER_UP	1.7090	4.316×10^{-6}
REACTOME_SIGNALING_BY_INTERLEUKINS	1.6783	6.083×10^{-6}
AMBROSINI_FLAVOPIRIDOL_TREATMENT_TP53	1.6697	6.761×10^{-6}
RICKMAN_TUMOR_DIFFERENTIATED_WELL_VS_MODERATELY_UP	1.6692	6.759×10^{-6}
JOSEPH_RESPONSE_TO_SODIUM_BUTYRATE_DN	1.6617	7.423×10^{-6}
JAEGER_METASTASIS_DN	1.6567	8.002×10^{-6}
REACTOME_CYTOCHROME_P450_ARRANGED_BY_SUBSTRATE_TYPE	1.6418	9.414×10^{-6}
SILIGAN_BOUND_BY_EWS_FLT1_FUSION	1.6418	9.411×10^{-6}
REACTOME_REGULATION_OF_LIPID_METABOLISM_BY_PPARALPHA	1.6418	9.408×10^{-6}
WANG_LMO4_TARGETS_UP	1.5653	2.3004×10^{-6}
SABATES_COLORECTAL_ADENOMA_UP	1.5647	2.914×10^{-5}
SERVITJA_LIVER_HNF1A_TARGETS_DN	1.5612	2.464×10^{-5}
SENESE_HDAC1_AND_HDAC2_TARGETS_UP	1.5224	3.946×10^{-5}
IWANAGA_CARCINOGENESIS_BY_KRAS_PTEN_DN	1.5019	4.511×10^{-5}
HAN_SATB1_TARGETS_UP	1.5008	4.589×10^{-5}
RICKMAN_HEAD_AND_NECK_CANCER_A	1.4944	4.887×10^{-5}
HOLLEMAN_VINCRISTINE_RESISTANCE_ALL_DN	1.4567	7.782×10^{-5}
ENK_UV_RESPONSE_EPIDERMIS_UP	1.4008	1.360×10^{-4}
REACTOME_METABOLISM_OF_LIPIDS	1.3783	1.807×10^{-4}
REACTOME_BIOLOGICAL_OXIDATIONS	1.3665	1.893×10^{-4}
REACTOME_PHASE_I_FUNCTIONALIZATION_OF_COMPOUNDS	1.3665	1.888×10^{-4}
HOELZEL_NF1_TARGETS_DN	1.3498	2.384×10^{-4}
TURASHVILI_BREAST_LOBULAR_CARCINOMA_VS_LOBULAR_NORMAL_UP	1.3439	2.445×10^{-4}
JAATINEN_HEMATOPOIETIC_STEM_CELL_DN	1.3406	2.483×10^{-4}
FARMER_BREAST_CANCER_APOCRINE_VS_LUMINAL	1.3296	2.761×10^{-4}
ACEVEDO_LIVER_CANCER_DN	1.3181	3.214×10^{-4}
MARTORIATI_MDM4_TARGETS_FETAL_LIVER_DN	1.3010	3.676×10^{-4}
ENK_UV_RESPONSE_EPIDERMIS_DN	1.2851	4.262×10^{-4}

Table 2.

Differentially enriched C2 genesin WT mouse DLPs upon *Ghr* deletion.

Gene Set name	log_2FoldChange	Corrected p-value
REACTOME_CYTOKINE_SIGNALING_IN_IMMUNE_SYSTEM	1.405405405	1.962×10^{-4}
ACEVEDO_LIVER_TUMOR_VS_NORMAL_ADJACENT_TISSUE_UP	1.399361967	2.080×10^{-4}
REACTOME_TRANSLATION	1.383204633	2.474×10^{-4}
REACTOME_EUKARYOTIC_TRANSLATION_INITIATION	1.383204633	2.475×10^{-4}
RHEIN_ALL_GLUCOCORTICOID_THERAPY_DN	1.375625626	2.692×10^{-4}
YAMASHITA_LIVER_CANCER_WITH_EPCAM_UP	1.375625626	2.693×10^{-4}
REACTOME_SELENOAMINO_ACID_METABOLISM	1.375625626	2.693×10^{-4}
GRAESSMANN_APOPTOSIS_BY_SERUM_DEPRIVATION_UP	1.349249249	3.466×10^{-4}
GRAESSMANN_RESPONSE_TO_MC_AND_SERUM_DEPRIVATION_UP	1.349249249	3.470×10^{-4}
RAY_TUMORIGENESIS_BY_ERBB2_CDC25A_DN	1.349249249	3.475×10^{-4}
PUJANA_BRCA1_PCC_NETWORK	1.330343222	4.253×10^{-4}
ACEVEDO_NORMAL_TISSUE_ADJACENT_TO_LIVER_TUMOR_DN	1.313738739	4.913×10^{-4}
GRAESSMANN_APOPTOSIS_BY_DOXORUBICIN_UP	1.313563564	4.989×10^{-4}
RAY_TUMORIGENESIS_BY_ERBB2_CDC25A_UP	−1.32307833	4.655×10^{-4}
PEDRIOLI_MIR31_TARGETS_DN	−1.329615792	4.242×10^{-4}
OSWALD_HEMATOPOIETIC_STEM_CELL_IN_COLLAGEN_GEL_UP	−1.417455808	1.733×10^{-4}